Supporting Information

Material Design of New p-Type Tin Oxyselenide Semiconductor through Valence Band Engineering and Its Device Application

Taikyu Kim,[†] Baekeun Yoo,[†] Yong Youn,[§] Miso Lee,[§] Aeran Song,[‡] Kwun-Bum Chung,[‡] Seungwu Han,[§] and Jae Kyeong Jeong[,†]*

†Department of Electronic Engineering, Hanyang University, Seoul 04763, Korea

§Department of Materials Science and Engineering and Research Institute of Advanced Materals, Seoul National University, Seoul 08826, Korea

‡Division of Physics and Semiconductor Science, Dongguk University, Seoul 04620, Korea

*E-mail: jkjeong1@hanyang.ac.kr

1. Cross-sectional SEM images of the SnO film with different oxygen partial pressure

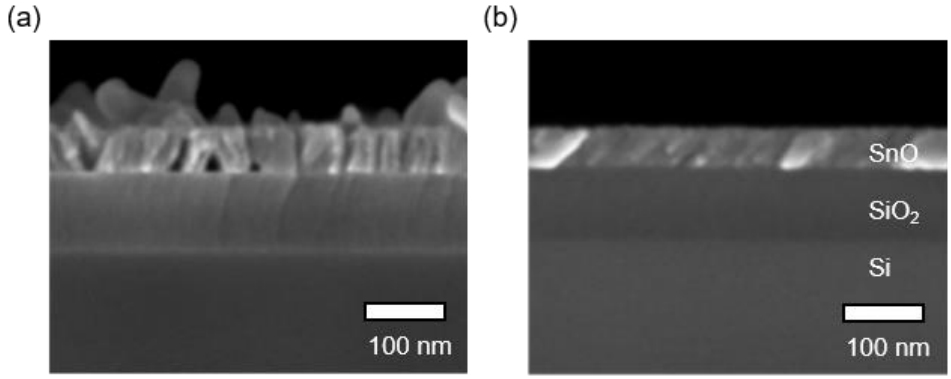

Figure S1. SEM micrographs of the annealed SnO films, which was grown at the oxygen partial pressure of (a) 4 % (left) and (b) 10 % (right) on SiO_2/Si substrates.

2. Plan-view TEM image of the $SnSe_{0.56}O_{0.44}$ film.

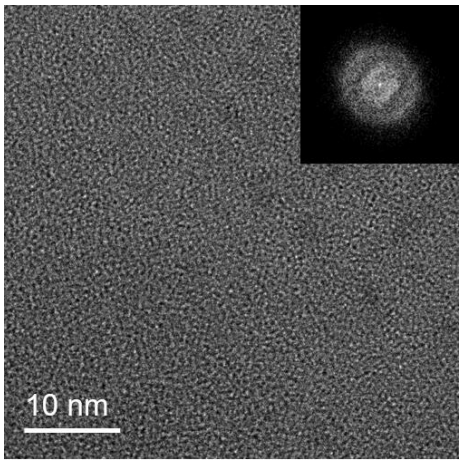

Figure S2. Plan-view TEM image of the $SnSe_{0.56}O_{0.44}$ film. The SADP of the $SnSe_{0.56}O_{0.44}$ film was shown as an inset, indicating the amorphous phase nature.

3. XPS Analysis of the Se 3d peak.

The following deconvolution of the XP spectra of selenium *3d* was based on the ref. 1.

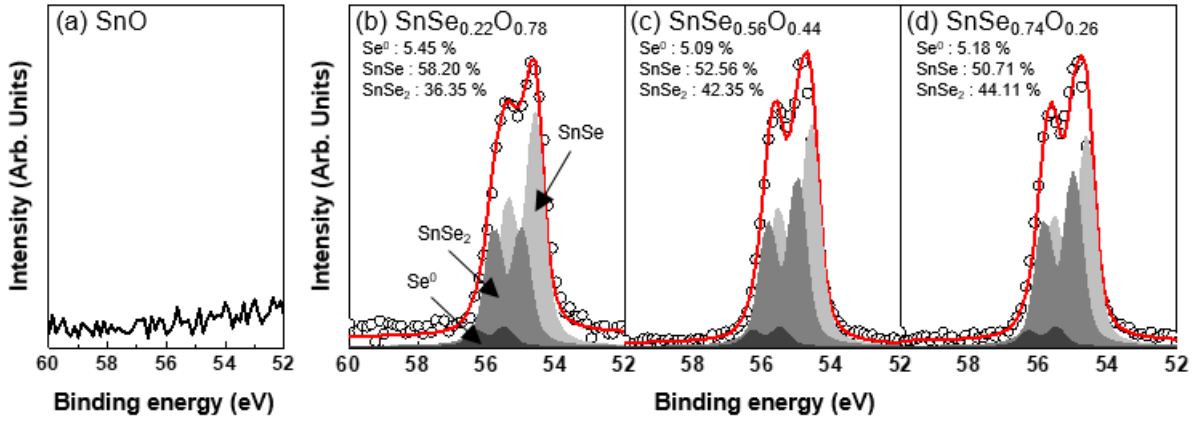

Figure S3. XP spectra of Se *3d* of (a) SnO, (b) $SnSe_{0.22}O_{0.78}$, (c) $SnSe_{0.56}O_{0.44}$ and (d) $SnSe_{0.74}O_{0.26}$ thin-films annealed at 300 °C. The binding energy states of the Se with three different bonds (SnSe, $SnSe_2$, and Se^0) corresponds to the peaks approximately 54.6, 55.0, and 55.5 eV, respectively.

4. Transmittance and band alignment of the $SnSe_xO_{1-x}$ films.

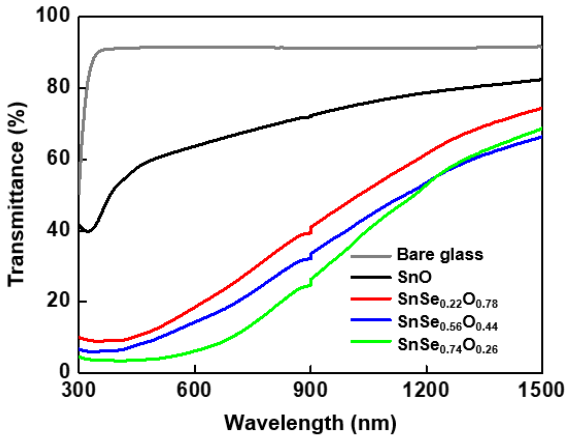

Figure S4. Transmittance of the 30 nm $SnSe_xO_{1-x}$ (x = 0, 0.22, 0.56, 0.74) thin films annealed at 300 C°.

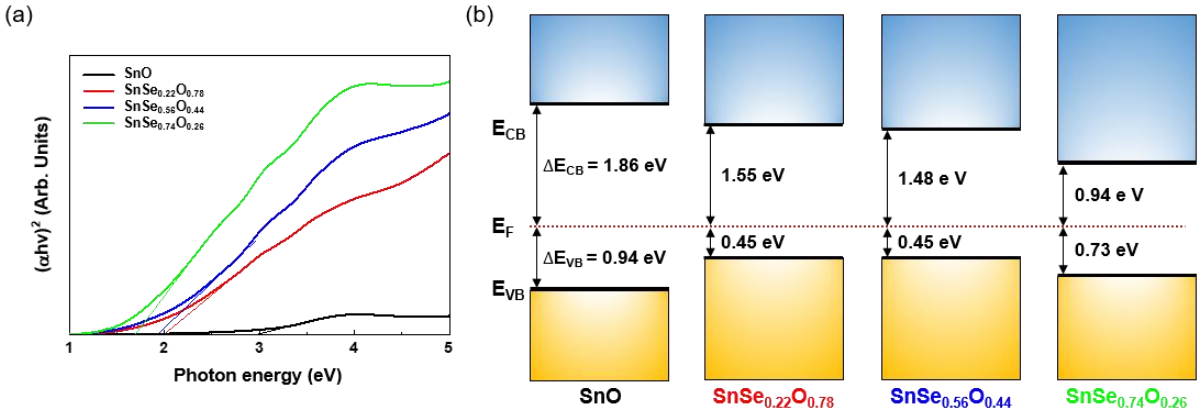

Figure S5. (a) Direct bandgap extracted from the absorption coefficient relative to the photon energy. (b) Band alignment of the $SnSe_xO_{1-x}$ (x = 0, 0.22, 0.56, 0.74) thin film.

5. I_{DS}-V_{GS} curve and V_{GS}-dependent field-effect mobility variation of the $SnSe_{0.56}O_{0.44}$ FETs.

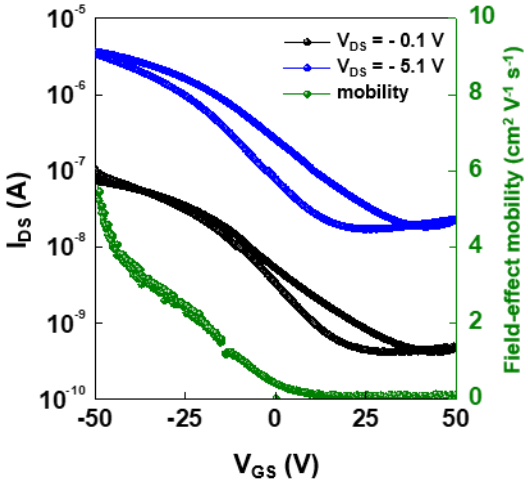

Figure S6. Transfer characteristics and variation in V_{GS}-dependent mobility of the $SnSe_{0.56}O_{0.44}$ FETs. I_{DS}-V_{GS} curves were measured in double-sweep gate voltage mode.

6. Electrical characteristics of the $SnSe_xO_{1-x}$ films and their FETs near x = 0.56.

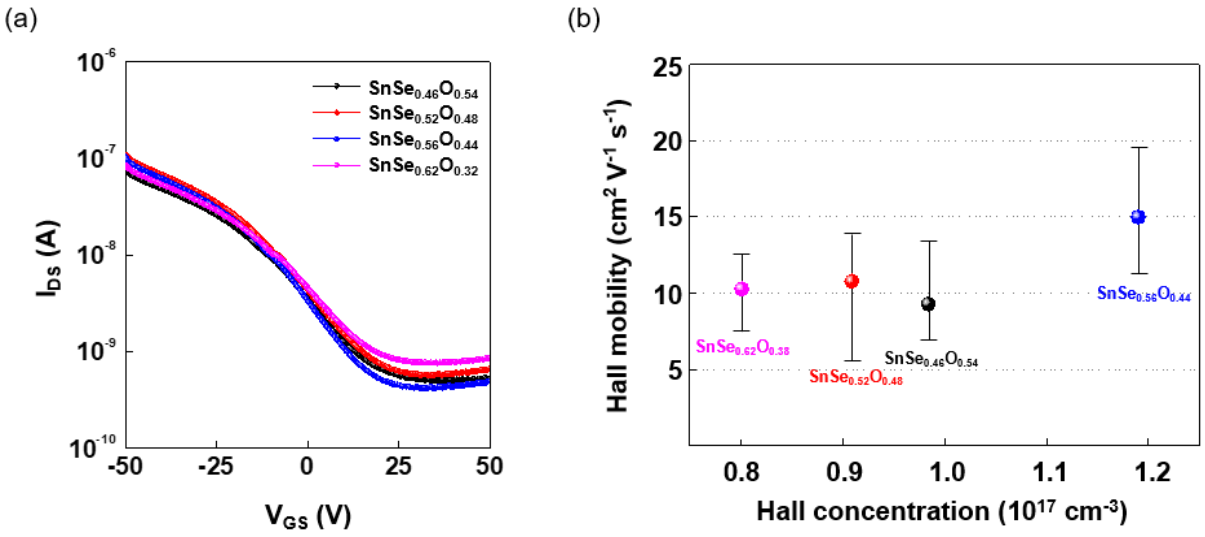

Figure S7. (a) Transfer characteristics of $SnSe_xO_{1-x}$ FETs with the Se fraction near x = 0.56. (b) Hall effect measurement of $SnSe_xO_{1-x}$ thin-films with the Se fraction near x = 0.56.

Table S1. Electrical parameters of the $SnSe_xO_{1-x}$ films and their FETs with Se fraction near x = 0.56.

	$SnSe_{0.46}O_{0.54}$	$SnSe_{0.52}O_{0.48}$	$SnSe_{0.56}O_{0.44}$	$SnSe_{0.62}O_{0.38}$
n_h [cm^{-3}]	9.8 x 10^{16}	9.1 x 10^{16}	1.2 x 10^{17}	8.0 x 10^{16}
μ_{hall} [$cm^2 V^{-1} s^{-1}$]	9.3 ± 2	10.8 ± 3	15.0 ± 4	10.3 ± 3
$I_{ON/OFF}$	2 x 10^2	2 x 10^2	3 x 10^2	1 x 10^2
μ_{FE} [$cm^2 V^{-1} s^{-1}$]	4.0	5.3	5.9	4.6

7. Comparison with several important p-type materials recently reported.

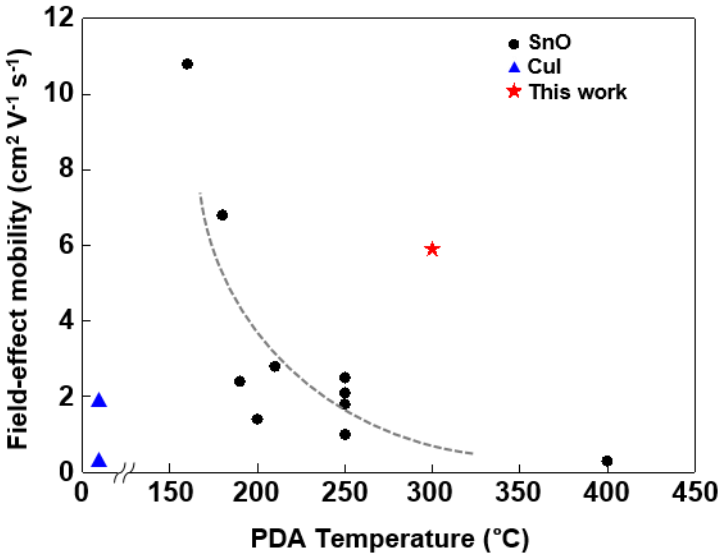

Figure S8. Relation between PDA temperature and field-effect mobilty for the high performance p-type SnO FETs, which was summaried from the **Table S2**. It includes the results for the solution-based CuI FETs, which were reported very recently. Most of high performance SnO FETs have been fabricated at $T_{PDA} \leq 250$ °C.

Table S2. Summary of performance of several important tin monoxide films and related FETs. The recently reported CuSnI and CuI thin film properties were also included.

	Gate Insulator[a]	Method[b]	T_{dep}[c] [℃]	T_{PDA}[d] [℃]	PDA time [min]	μ_{hall} [$cm^2V^{-1}s^{-1}$]	n_h [cm^{-3}]	μ_{FE} [$cm^2V^{-1}s^{-1}$]	Year	Ref
SnO	SiO_2	EBE	RT	400	10	-	-	0.3	2012	[2]
SnO	SiO_2	EBE	RT	400	10	-	-	0.3	2012	[3]
SnO	SiO_2	RFMS	RT	250	60	3	1.0×10^{18}	1.8	2013	[4]
SnO	HfO_2	DCMS	RT	160	30	-	-	10.8	2013	[5]
SnO	HfO_2	DCMS	RT	180	30	18.7	2.2×10^{17}	6.8	2013	[6]
SnO	YSZ	PLD	575	-	-	7	1.0×10^{17}	-	2013	[7]
SnO	HfO_2	RFMS	RT	250	60	-	-	2.1	2014	[8]
SnO	SiO_x	RFMS	90	-	-	-	-	4.9	2014	[9]
SnO	SiO_2	RFMS	RT	200	120	1.4	7.0×10^{17}	1.4	2014	[10]
SnO	SiO_2	PLD	500	-	-	2	9.0×10^{16}	0.3	2015	[11]
SnO	ATO	DCMS	RT	190	30	-	-	2.4	2015	[12]
SnO	SiO_2	RFMS	RT	250	100 sec	-	-	1.8	2015	[13]
SnO	SiO_2	DCMS	RT	210	60	5.5	1.8×10^{18}	2.8	2016	[14]
SnO	SiO_2	ALD	210	250	60	-	-	1.0	2017	[15]
SnO	ZrO_2	DCMS	RT	250	60	-	-	2.5	2017	[16]
SnO	Al_2O_3	TE	250	-	-	-	-	1.4	2018	[17]
CuSnI	PET	SC	140	-	-	8.9	4.0×10^{18}	-	2018	[18]
CuI	SiO_2	SC	RT	-	-	5.1	5.0×10^{19}	0.44	2018	[19]
CuI	ZrO_2	SC	RT	-	-	5.1	5.0×10^{19}	1.9	2018	[19]
SnSeO	SiO_2	DCMS	RT	300	60	15.0	1.2×10^{17}	5.9	2019	This work

(a) Gate Insulator: Gate insulator used in the Hall measurement or FETs. (YSZ: yttria stabilized zirconia. ATO: superlattice of TiO_2 and Al_2O_3); [b]Method: the deposition method for the channel layer. (EBE: electron-beam evaporation. RFMS: radio-frequency magnetron sputtering. DCMS: direct current magnetron sputtering. PLD: pulsed laser deposition. ALD: atomic layer deposition. TE: thermal evaporation. SC: spin coating); [c]T_{dep} and [d]T_{PDA}: temperature during the deposition and post deposition annealing process, respectively.

8. Comparison of thermal stability between the SnO and $SnSe_{0.56}O_{0.44}$ FETs.

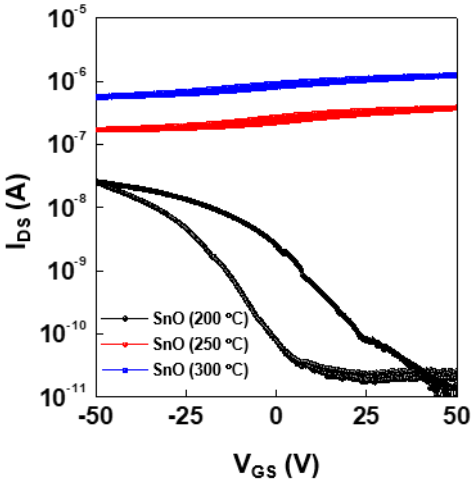

Figure S9. Transfer characteristics of the SnO FETs annealed at different temperatures of 200, 250 and 300 °C. I_{DS}-V_{GS} curves were measured at V_{DS} = - 0.1 V.

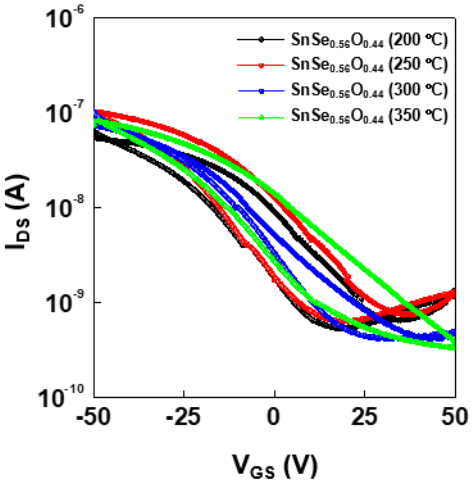

Figure S10. Transfer characteristics of the $SnSe_{0.56}O_{0.44}$ FETs annealed at different temperatures (200, 250, 300 and 350 °C). I_{DS}-V_{GS} curves were measured at V_{DS} = - 0.1 V.

9. Transfer characteristics of the n-type IGZO FETs for CMOS inverter.

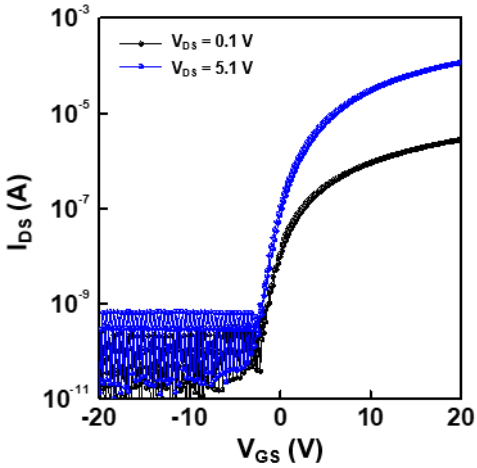

Figure S11. Transfer characteristics of the n-type IGZO FETs adopted for the complementary metal oxide semiconductors.

10. I_{DS}-V_{GS} curves of the $SnSe_xO_{1-x}$ FETs in double-sweep gate voltage mode.

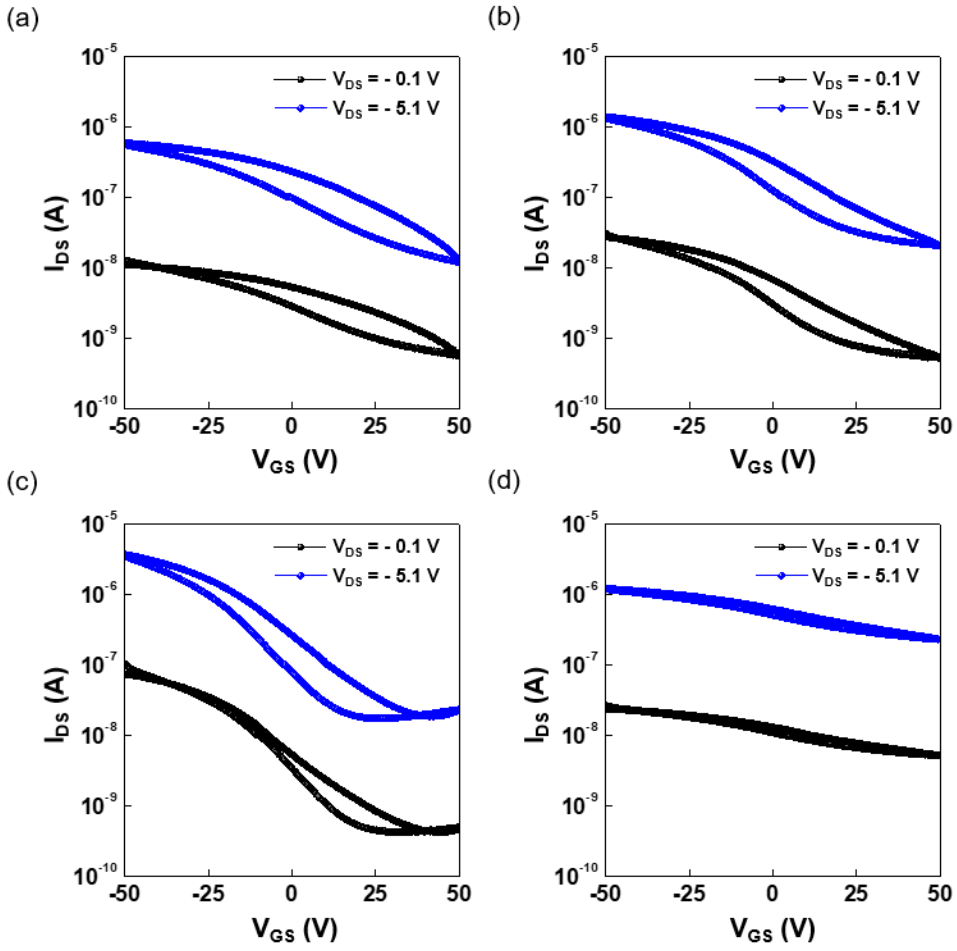

Figure S12. Transfer characteristics of the (a) control SnO, (b) $SnSe_{0.22}O_{0.78}$, (c) $SnSe_{0.56}O_{0.44}$ and (d) $SnSe_{0.74}O_{0.26}$ FETs annealed at 300 °C, which were measured in double-sweep gate voltage mode.

REFERENCES

[1] Vishwanath, S.; Liu, X.; Rouvimov, S.; Basile, L.; Lu, N.; Azcatl, A.; Magno, K.; Wallace, R. M.; Kim, M.; Idrobo, J.-C.; Furdyna, J. K.; Jena, D.; Xing, H. G. Controllable Growth of Layered Selenide and Telluride Heterostructures and Superlattices Using Molecular Beam Epitaxy. *J. Mater. Res.* **2016**, 31, 900-910.

[2] Liang, L.; Cao, H. Ambipolar SnO Thin-Film Transistors and Inverters. *ECS Trans*. **2013**, 50, 289-297.

[3] Liang, L. Y; Cao, H. T.; Chen, X. B.; Liu, Z. M.; Zhuge, F.; Luo, H.; Li, J.; Lu, Y. C.; Lu, W. Ambipolar Inverters Using SnO Thin-Film Transistors with Balanced Electron and Hole Mobilities. *Appl. Phys. Lett.* **2012**, 100, 263502.

[4] Hsu, P. C.; Chen, W. C.; Tsai, Y. T.; Kung, Y. C.; Chang, C. H.; Hsu, C. J.; Wu, C. C.; Hsieh, H. H. Fabrication of p-Type SnO Thin-Film Transistors by Sputtering with Practical Metal Electrodes. *Jpn. J. Appl. Phys*. **2013**, 52, 5S1.

[5] Caraveo-Frescas, J. A.; Alshareef, H. N. Transparent p-Type SnO Nanowired with Unprecedented Hole Mobility among Oxide Semiconductors. *Appl. Phys. Lett.* **2013**, 103, 222103.

[6] Caraveo-Frescas, J. A.; Nayak, P. K.; Al-Jawhari, H. A.; Granato, D. B.; Schwingenschlogl, U.; Alshareef, H. N. Record Mobility in Transparent p-Type Tin Monoxide Films and Devices by Phase Engineering. *ACS Nano* **2013**, 7, 5160-5167.

[7] Quackenbush, N. F.; Allen, J. P.; Scanlon, D. O.; Sallis, S.; Hewlett, J. A.; Nandur, A. S.; Chen, B.; Smith, K. E.; Weiland, C.; Fischer, D. A.; Woicik, J. C.; White, B. E.; Watson, G. W.; Piper, L. F. J. Origin of the Bipolar Doping Behavior of SnO from X-ray Spectroscopy and Density Functional Theory. *Chem. Mater.* **2013**, 25, 3114-3123.

[8] Chiu, I. C.; Cheng, I. C. Gate-Bias Stress Stability of p-Type SnO Thin-Film Transistors Fabricated by RF-Sputtering. *IEEE Electron Device Lett*. **2014**, 35, 90-92.

[9] U, M.; Han, Y.-J.; Song, S.-H.; Cho, I.-T.; Lee, J.-H.; Kwon, H.-I. High Performance p-Type SnO Thin-Film Transistor with SiO_x Gate Insulator Deposited by Low-Temperature PECVD Method. *J. Semicond. Technol. Sci*. **2014**, 14, 666-672.

[10] Luo, H.; Liang, L. Y.; Liu, Q.; Cao, H. T. Magnetron-Sputtered SnO Thin Films for p-Type and Ambipolar TFT Applications. *ECS J. Solid State Sci. Technol*. **2014**, 3, Q3091-Q3094.

[11] Liao, M.; Xiao, Z. W.; Ran, F. Y.; Kumomi, H.; Kamiya, T.; Hosono, H. Effects of Pb Doping on Hole Transport Properties and Thin-Film Transistor Characteristics of SnO Thin Films. *ECS J. Solid State Sci. Technol.* **2015**, 4, Q26-Q30.

[12] Wang, Z.; Al-Jawhari, H. A.; Nayak, P. K.; Caraveo-Frescas, J. A.; Wei, N.; Hedhili, M. N.; Alshareef, H. N. Low Temperature Processed Complementary Metal Oxide Semiconductor (CMOS) Device by Oxidation Effect from Capping Layer. *Sci. Rep*. **2015**, 5, 9617.

[13] Han, Y.-J.; Choi, Y.-J.; Jeong, C.-Y.; Lee, D.; Song, S.-H.; Kwon, H.-I. Environment-Dependent Bias Stress Stability of p-Type SnO Thin-Film Transistors. *IEEE Electron Device Lett*. **2015**, 36, 466-468.

[14] Han, S. J.; Kim, S.; Ahn. J.; Jeong, J. K.; Yang, H.; Kim, H. J. Composition-Dependent Structural and Electrical Properties of p-Type SnO_x Thin Films Prepared by Reactive DC Magnetron Sputtering: Effects of Oxygen Pressure and Heat Treatment. *RSC Advances* **2016**, 6, 71757-71766.

[15] Kim, S. Y.; Baek, I. H.; Kim, D. H.; Pyeon, J. J.; Chung, T. M.; Baek, S. H.; Kim, J. S.; Han, J. H.; Kim, S. K. Fabrication of High-Performance p-Type Thin Film Transistors Using Atomic-Layer-deposited SnO Films. *J. Mater. Chem. C* **2017**, 5, 3139-3145.

[16] Azmi, A.; Lee, J.; Gim, T. J.; Choi, R.; Jeong, J. K. Performance Improvement of p-Channel Tin Monoxide Transistors with a Solution-Processed Zirconium Oxide Gate Dielectric. *IEEE Electron Device Lett.* **2017**, 38, 1543-1546.

[17] Hung, M. P.; Genoe, J.; Heremans, P.; Steudel, S. Off-Current Reduction in p-Type SnO Thin Film Transistors. *Appl. Phys. Lett*. **2018**, 112, 263502.

[18] Jun, T.; Kim, J.; Sasase, M.; Hosono, H. Material Design of p-Type Transparent Amorphous Semiconductor, Cu-Sn-I. *Adv. Mater*. **2018**, 30, 1706573.

[19] Liu, A.; Zhu, H.; Park, W. T.; Kang, S. J.; Xu, Y.; Kim, M. G.; Noh, Y. Y. Room-Temperature Solution-Synthesized p-Type Copper (I) Iodide Semiconductors for Transparent Thin-Film Transistors and Complementary Electronics. *Adv. Mater*. **2018**, 30, 1802379.